Sensititity of the stability threshold in linearized rotordynamics

B.Vervisch [1,2]**,K.Stockman** [1,2]**, M.Loccufier** [2]
[1] Technical University of West-Flanders, Department of Electromechanical Engineering,
Graaf Karel de Goedelaan 5, B-8500, Kortrijk, Belgium
e-mail: **bram.vervisch@howest.be**

[2] University of Ghent, Departement of Electrical Engineering, Systems and Automation
Technologiepark 914, B-9052, Zwijnaarde, Belgium

Abstract
Rotors exposed to lateral vibration can become unstable at a certain speed due to rotor internal damping. This stability threshold speed is unique and it is impossible to rotate above the threshold. In this paper, a rotor is treated as a linear speed dependent system and inertia, stiffness, gyroscopic and damping forces are included. In order to find the stability threshold, the multiple degree of freedom equations of motion are decoupled into a set of scalar equations. Therefore, the quadratic eigenvalue problem has to be solved. Consequently, the stability threshold speed can be calculated as the lowest speed by which one of the roots has a positive real part. The parameters that influence this stability threshold are discussed and verified by numerical results.

1 Introduction

Self-excited vibrations have been a field of study in linearized rotordynamics, for over a century. Ever since De Laval proved experimentally in 1895 that turbines can operate supercritically, in order to increase performance for lower dimensions, manufacturers became aware of severe vibrations and instabilities when operating at this speed. Nowadays, high speed, high performance and reliable rotating machinery play an important role in many industries going from power generation to manufacturing and even home appliances [1]. To satisfy all these expectations, an accurate knowledge of the stability threshold is required. Besides the widely known oil whirl and whip phenomenon induced by hydrodynamic bearings, rotor internal damping is recognized as one of the main causes of self-excited vibrations [2]. This type of damping induces a follower force, increasing the whirling amplitude in the supercritical field. It is shown theoretically that the whirling motion of the rotor becomes unstable at all speeds above the stability threshold and that this threshold is always larger than the corresponding whirling speed [3]. However, the stability threshold is highly dependent on the model structure and in order to get a realistic estimation, the model should include all the forces that affect this threshold. These are typically inertia, stiffness, gyroscopic and damping forces. On the contrary, in the industry, a model should be as simplified as possible to gain insight and to reduce computational time. Therefore a model that is linear and time invariant for a fixed speed is preferred in rotordynamics. This type of model is usually the result of a discretization technique such as finite elements [4].
In this paper, the sensitivity of the stability threshold is studied for these kinds of models. Therefore, the quadratic eigenvalue problem is solved[5]. Because of the impossibility to rotate above the stability threshold, the actual threshold will be the one with the lowest speed. It is widely known that for an undamped non-rotating system, the eigenvalues and their corresponding eigenvectors have a specific ordering which is characterized by Rayleigh's coefficient. As long as the system has specific properties, a similar technique can be used to study the effect of the eigenvectors on the stability threshold. Otherwise, only experimental

validation can give a solution.
In section two, the equations of motion for the linear speed dependent model and the choice for complex coordinates are explained. Subsequently, section three discusses the matrices of the finite element model with a special focus on the damping matrix containing either viscous damping, hysteretic damping or a combination of both. Taking this into account, the stability threshold speed is calculated for a system that is uncoupled by its eigenvectors in section four. With this method, the stability threshold speed is defined by five parameters. These parameters can also lead to a Campbell diagram and a decay rate plot. In a similar way, the ordering of the stability threshold is questioned. Finally, in section five, the theory is illustrated with numerical results.

2 Equations of motion

2.1 The linear speed dependent model

Whereas rotating structures are generally nonlinear and continuous, this kind of system is mostly linearized and discretized. However, this linearization is only valid under the assumption that the vibrations are small and the accuracy of the discretization technique will only be sufficient if enough elements are chosen; a widely used concept. As a result, typical equations of motion are obtained containing a mass matrix, $\mathbf{M}$, a damping matrix, $\mathbf{C}$, and stiffness matrix, $\mathbf{K}$. However, due to rotation, some of the properties change periodically in time, thus, the matrices become time dependent [6].

$$\mathbf{M}(t)\ddot{\mathbf{q}} + \mathbf{C}(t)\dot{\mathbf{q}} + \mathbf{K}(t)\mathbf{q} = \mathbf{f}(t), \quad \mathbf{q}(t), \mathbf{f}(t) \in \mathbb{R}^n \tag{1}$$

with n, the degrees of freedom. In most rotating machinery, the structure is commonly assumed to contain only isotropic rotating elements with properties invarient in time. Under these assumptions, the matrix properties are no longer time depentent, but only speed dependent and equation (1) can be simplified:

$$\mathbf{M}(\Omega)\ddot{\mathbf{q}} + \mathbf{C}(\Omega)\dot{\mathbf{q}} + \mathbf{K}(\Omega)\mathbf{q} = \mathbf{f}(t), \quad \mathbf{q}(t), \mathbf{f} \in \mathbb{R}^n \tag{2}$$

with Ω the rotating speed. In non-rotating structures, the mass matrix and the stiffness matrix represent respectively the conservative inertial and stiffness forces, while the damping matrix represents the non-conservative damping forces. In rotating structures these properties are mixed resulting in a combination of conservative and non-conservative forces in both the damping and stiffness matrix [1]. For this reason the matrix $\mathbf{C}$ is sometimes called the velocity dependent matrix and $\mathbf{K}$, the displacement dependent matrix [7]. This terminology is used throughout this paper.

2.2 Complex coordinates

Independent of the discretization technique for a fixed rotation axis, every discrete node in the rotating system has four degrees of freedom: two translations (v_i,w_i) and two rotations (ϕ_{yi}, ϕ_{zi}) (Figure 1). Whenever the rotor is axi-symmetrical, complex coordinates can be used [3].

$$\mathbf{q}_i = \begin{bmatrix} r_i \\ \phi_i \end{bmatrix} = \begin{bmatrix} v_i + iw_i \\ \phi_{yi} - i\phi_{zi} \end{bmatrix} \qquad i = \sqrt{-1} \tag{3}$$

The use of complex coordinates is very expedient in axi-symmetrical systems. It allows to study the system using a model whose size is just half the size of the same problem expressed in real coordinates[4]. Therefore, complex coordinates will be used in the remainder of the paper.

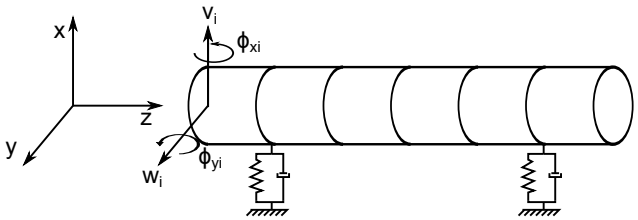

Figure 1: Schematic representation of the shaft on bearings divided in finite elements with four degrees of freedom per node

3 Discussion of the matrices

Mass, stiffness and gyroscopic matrices are usually derived from the kinetic and potential energy expression. Depending on the model resolution accuracy a lumped, distributed or consistent mass discretization can be used, whereas the consistent mass matrix appears to be slightly better for most cases [8]. The modeling of damping is not so straightforward. Usually, proportional damping is used which results in a viscous behaviour. Otherwise hysteretic damping can be incorporated using complex stiffness. A combination of both is also possible.

3.1 Mass, stiffness and gyroscopic matrices

For the modeling of the mass, stiffness and gyroscopic matrices, a finite element model is used based on the Euler-Bernouilli beam theory. This means that the shear deformation is not taken into account. It has two nodes at both ends of the beam and six degrees of freedom per node. Because only lateral vibrations are considered, the degrees of freedom reduce to four. This matrices result in

$$\mathbf{K}_{el} = \frac{EI}{l^3}\begin{bmatrix} 12 & 6l & -12 & 6l \\ & 4l^2 & -6l & 2l^2 \\ & & 12 & -6l \\ & symm & & 4l^2 \end{bmatrix} \tag{4}$$

$$\mathbf{M}_{Tel} = \frac{\rho Al}{420}\begin{bmatrix} 156 & l22 & 54 & -13l \\ & 4l^2 & l13 & -3l^2 \\ & & 156 & -22l \\ & symm & & 4l^2 \end{bmatrix} \tag{5}$$

$$\mathbf{M}_{Rel} = \frac{\rho I}{30l}\begin{bmatrix} 36 & l3 & 36 & -3l \\ & 4l^2 & l3 & -1l^2 \\ & & 36 & -3l \\ & symm & & 4l^2 \end{bmatrix} \tag{6}$$

and

$$\mathbf{M}_{el} = \mathbf{M}_{Tel} + \mathbf{M}_{Rel}, \quad \mathbf{G}_{el} = 2\mathbf{M}_{Rel} \tag{7}$$

With $\mathbf{K}_{el}$, $\mathbf{M}_{Tel}$ and $\mathbf{M}_{Rel}$ respectively the stiffness, translational mass and rotational mass matrix. $\mathbf{M}_{el}$ and $\mathbf{G}_{el}$ are the mass and the gyroscopic matrix. The stiffness of the bearings is taken into account as linear springs on the nodes affecting both translation and rotation (Figure 1).

3.2 Damping matrices

3.2.1 Viscous damping

The damping matrices can be modeled in a proportional way if purely viscous damping is assumed. Proportional damping is defined as

$$\mathbf{C}_{n0} = a\mathbf{K}_{b0} + b\mathbf{M} \tag{8}$$
$$\mathbf{C}_{r0} = a\mathbf{K}_{r0} + b\mathbf{M} \tag{9}$$

with $\mathbf{K}_{b0}$ containing the stiffness of the bearings and $\mathbf{K}_{r0}$ the stiffness of the shaft. Usually, however, a damping coefficient is used to define the damping[9][3]. This both leads to matrices proportional to the stiffness matrix only.

$$\mathbf{C}_{n0} = \eta_b\mathbf{K}_{b0} \tag{10}$$
$$\mathbf{C}_{r0} = \eta_v\mathbf{K}_{r0} \tag{11}$$

with η_b and η_v the viscous loss factor for the bearings and the shaft. Because the shaft is rotating, the viscous damping $\mathbf{C}_{r0}$ acts in both the nonrotating and rotating frame. This results in both an influence in the velocity dependent matrix $\mathbf{C}(\Omega)$ and the displacement dependent matrix $\mathbf{K}(\Omega)$. Moreover, the latter introduces a rotating speed dependency of the form $\Omega\mathbf{C}_{r0}$.
Viscous damping is easy to use but does not really have a physical interpretation. Therefore, hysteretic damping can be used as an alternative.

3.2.2 Hysteretic damping

When the shaft is whirling, with a whirling speed ω, bending will occur. This means that the shaft will be exposed to strain related stresses. In linear theory, the stress-strain relation of the shaft material involves a damping force which is proportional to the first derivative of the strain, in contrast to the restoring force which is proportional to the strain itself. Thus, there is a 90°phase difference between the damping force and the restoring force [10]. In Figure 2 the section of a shaft is depicted for three different situations: one synchronous whirl in Figure 2b, with $\Omega = \omega$, and two asynchronous whirls in Figure 2a, with $\Omega < \omega$, and in Figure 2c, with $\Omega > \omega$. In all three cases, the forces that act on the shaft are different.
At first, if $\Omega = \omega$, the shaft will bend once and then remain in its initial state, so the strain rate of change will be zero. As a result, the damping force will be zero. Secondly, if $\Omega < \omega$, the material at point one is traveling from being compressed at t_1 to stretched at t_4 in the opposite direction of the whirling speed. This results in a damping force that opposes the whirling speed, so damping will occur. Thirdly, if $\Omega > \omega$, the material at point one is traveling from compressed to stretched in the same direction of the whirling speed. This results in a damping force that enforces the whirling speed, so the system will become unstable. Furthermore, it should be noted that there is a sign change in the damping force when passing a whirling speed.

Because of the observation that the energy losses in engineering materials undergoing cyclic loading are proportional to the square of the displacement amplitude and almost independent of frequency [11], hysteretic damping is included as a frequency independent matrix. It can be incorporated in the model by introducing a hysteretic loss factor η_h [9][3].

$$\mathbf{C}_{h0} = \left(\frac{1+\eta_h}{\sqrt{1+\eta_h^2}} \pm i\frac{\eta_h}{\sqrt{1+\eta_h^2}} \right) \mathbf{K}_{r0} \tag{12}$$

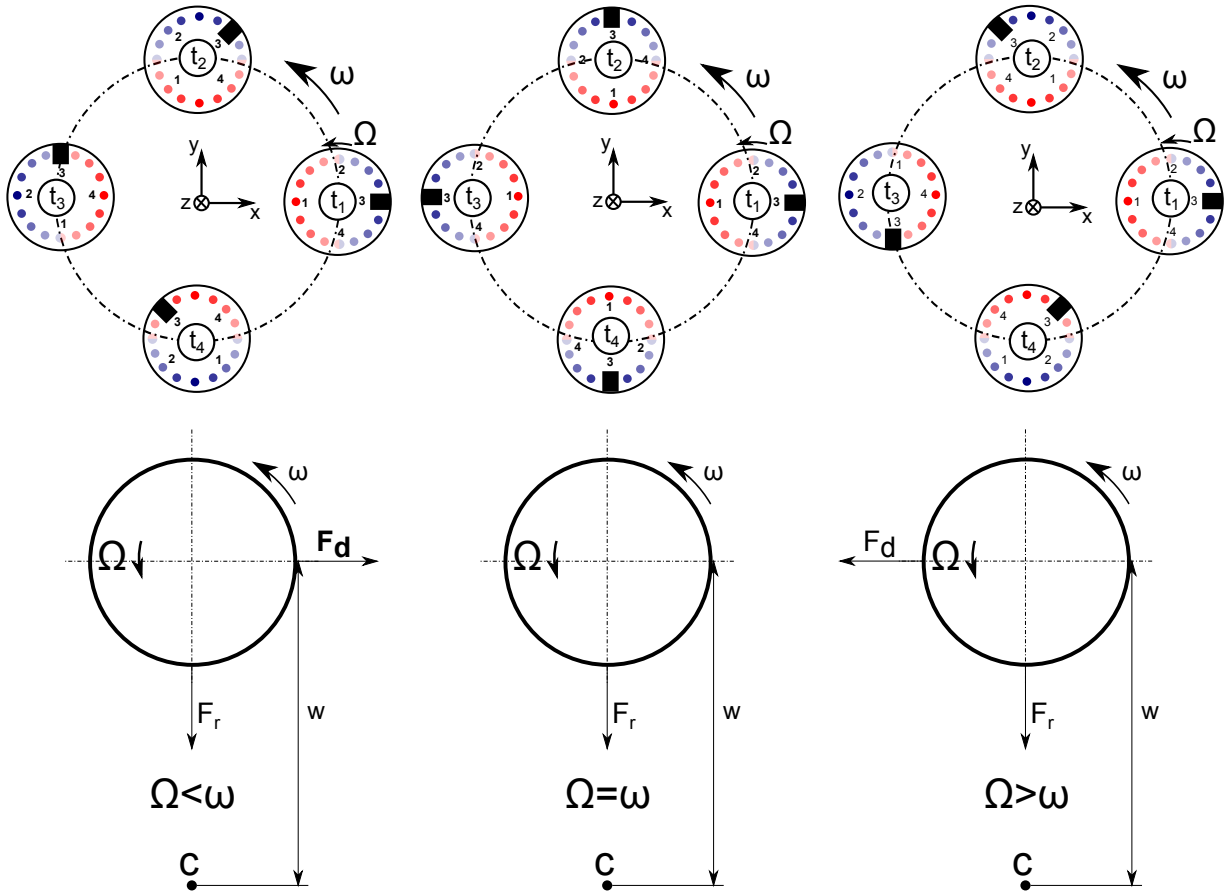

(a) Rotating speed < whirling speed (b) Rotating speed = speed (c) Rotating speed > whirling speed

Figure 2: Section of a shaft that is exposed to whirling

Because $\eta_h^2 << 1$ this can be approximated by

$$\mathbf{C}_{h0} = (1 + \eta_h \pm i\eta_h)\,\mathbf{K}_{r0} \tag{13}$$

The sign change of the imaginary part depends on the rotating speed, as explained above. Because of the complex coordinates, it is negative when $\Omega < \omega$ and positive when $\Omega > \omega$.
The disadvantage of this type of modeling is that it can only be used in systems with harmonic motion.

3.3 System equations

By the modeling choice explained above, equation (2) becomes

$$\mathbf{M}\ddot{\mathbf{q}} + (\eta_b \mathbf{K}_{b0} + \eta_v \mathbf{K}_{r0} - i\Omega \mathbf{G}_0)\,\dot{\mathbf{q}} + \left[\underbrace{\mathbf{K}_{r0} + \mathbf{K}_{b0} + \eta_h \mathbf{K}_{r0}}_{\mathbf{K}_0} - i\,(\Omega\eta_v \pm \eta_h)\,\mathbf{K}_{r0}\right]\mathbf{q} = 0 \tag{14}$$

where $\mathbf{q}$ is an n-dimensional vector containing the generalized coordinates [4]. This model includes inertial, stiffness, gyroscopic and damping forces. Centrifugal stiffening is neglected, the rotor is balanced and no external forces are observed. $\mathbf{M}$ represents the mass matrix, $\mathbf{K}_{r0}$ and $\mathbf{K}_{b0}$ the stiffness matrix of respectively the shaft and the bearings. The gyroscopic matrix, $\mathbf{G}_0$, represents the gyroscopic forces. Due to the complex

coordinates, all matrices are considered to be symmetric. In order to simplify further derivations, (14) is rewritten as

$$\mathbf{M}\ddot{\mathbf{q}} + \left(\mathbf{C}_{n0} + \mathbf{C}_{r0} - i\Omega\mathbf{G}_0\right)\dot{\mathbf{q}} + \left[\mathbf{K}_0 - i\left(\Omega\mathbf{C}_{r0} \pm \mathbf{C}_{h0}\right)\right]\mathbf{q} = 0 \tag{15}$$

4 The stability threshold

4.1 Stability threshold speed

For the system in (18) a nonsingular linear transformation $\mathbf{y} = \mathbf{Tq}$ exists such that it can be rewritten as follows [12]:

$$\ddot{\mathbf{y}} + \left(\mathbf{C}_{n0} + \mathbf{C}_{r0} - i\Omega\mathbf{G}\right)\dot{\mathbf{y}} + \left[\mathbf{K}_0 - i\left(\Omega\mathbf{C}_{r0} \pm \mathbf{C}_{h0}\right)\right]\mathbf{y} = 0 \tag{16}$$

where $K = diag(\lambda_1, \lambda_2, ..., \lambda_n)$ are the roots of the equation

$$det(\mathbf{M}\lambda - \mathbf{K}_0) = 0 \tag{17}$$

If $\mathbf{y} = \mathbf{u}e^{\mu t}$ is a solution of the equation, a quadratic eigenvalue problem is formed

$$\left\{\mu^2 + \left(\mathbf{C}_n + \mathbf{C}_r - i\Omega\mathbf{G}\right)\mu + \left[\mathbf{K} - i\left(\Omega\mathbf{C}_r \pm \mathbf{C}_h\right)\right]\right\}\mathbf{u} = 0 \tag{18}$$

The solution of this problem gives rise to 4n eigenvalues μ_i and their corresponding eigenvectors $\mathbf{u}_i$. The eigenvalues are of the form

$$\mu = \sigma + i\omega \tag{19}$$

where σ is the damping coefficient or the decay rate, and ω is the damped natural frequency. If equation (18) is premultiplied by its complex conjugate eigenvector $\overline{\mathbf{u}}^T$, a scalar equation is obtained [3][1]

$$\mu^2 + \left(c_n + c_r - i\Omega g\right)\mu + k - i\left(\Omega c_r \pm c_h\right) = 0 \tag{20}$$

The vector $\mathbf{u}$, defined by an arbitrary constant, is chosen such that $\mathbf{u}^*\mathbf{u} = 1$. Due to the matrix properties the scalars c_n, c_r, g, c_h and k are all real and positive and defined by

$$\mathbf{u}^*\mathbf{K}\mathbf{u} = k > 0 \tag{21}$$

$$\mathbf{u}^*\mathbf{C}_r\mathbf{u} = c_r \geq 0 \tag{22}$$

$$\mathbf{u}^*\mathbf{C}_h\mathbf{u} = c_h \geq 0 \tag{23}$$

$$\mathbf{u}^*\mathbf{C}_n\mathbf{u} = c_n \geq 0 \tag{24}$$

$$\mathbf{u}^*\mathbf{G}\mathbf{u} = g \geq 0 \tag{25}$$

In order to find the stability threshold, σ has to become positive. Consequently the stability threshold can be defined as the whirl speed by which the real part becomes zero. The means that the roots of equation (20) reduce to

$$\mu = i\omega \tag{26}$$

Substituting (26) in (20)

$$-\omega^2 + i(c_n + c_r)\omega + g\omega\Omega + k - i\left(c_r\Omega \pm c_h\right) = 0 \tag{27}$$

This can be separated into its real and imaginary parts

$$-\omega^2 + g\omega\Omega + k = 0 \tag{28}$$

$$(c_n + c_r)\omega - c_r\Omega \pm c_h = 0 \tag{29}$$

From equation (29) it is clear that the stability threshold Ω_s is

$$\Omega_s = \omega_s\left(1 + \frac{c_n}{c_r}\right) \pm \frac{c_h}{c_r} \tag{30}$$

The corresponding whirl speed, ω_s is

$$\omega_s = \left[\pm\frac{gc_h}{c_r} \pm \sqrt{\left(\frac{gc_h}{c_r}\right)^2 - 4k\left[g\left(1 + \frac{c_n}{c_r}\right) - 1\right]}\right]\left[\frac{1}{2g\left(1 + \frac{c_n}{c_r}\right) - 2}\right] \tag{31}$$

From equation (30) and inequalities (22) and (23) it is clear that the sign of Ω_s should always be the same as the one of ω. Moreover, the sign of Ω_s is positive, as chosen by the user. This means that in (31) only the positive ω_s is an existing solution and the stability threshold speed is a forward whirling speed. It can be concluded that all backward modes are stable. Furthermore, because there are 4n eigenvectors, there are 4n equations like (20) each with there own quantities (21-24). It can be said that every mode has a potential stability threshold speed. Nevertheless, it is shown that it is impossible to rotate above the stability threshold [3]. As a result, there will only be one threshold, in fact the lowest value of (30).

4.2 Decay rate plot of parameters

Parameters (21-25) can not only be used to calculate the stability threshold speed, but also to visualize the trend of the poles as a function of the rotating speed. Typically this is done by a Campbell diagram and a decay rate plot. Therefore, (20) is solved for μ

$$\mu = -\frac{c_n + c_r - ig\Omega}{2} \pm \sqrt{(c_n + c_r - ig\Omega)^2 - 4\left[k - i\left(\Omega c_r \pm c_h\right)\right]} \tag{32}$$

By splitting this into its real and imaginary part, respectively the decay rate plot and the Campbell diagram can be calculated. If

$$a = (c_n + c_r)^2 + g^2\Omega^2 - 4k \tag{33}$$

$$b = -2g\Omega(c_n + c_r) + 4\left(\Omega c_r \pm c_h\right) \tag{34}$$

The real part of the poles, σ, and the imaginary part, ω, can be written as

$$\sigma(\Omega) = Re(\mu(\Omega)) = -\frac{c_n + c_r}{2} \pm \frac{1}{2}\sqrt{a + \sqrt{\frac{a^2 + b^2}{2}}} \tag{35}$$

$$\omega(\Omega) = Im(\mu(\Omega)) = \frac{g\Omega}{2} \pm \frac{1}{2}sgn(b)\sqrt{-a + \sqrt{\frac{a^2 + b^2}{2}}} \tag{36}$$

Considering the sign change in c_h, it should be noted that the sign of b can also change. This has an effect on (36). One should always take into account to chose the right ω with the corresponding σ. Because both Campbell diagram and decay rate plot are expressed by the parameters (21-25), they are called the Campbell diagram and the decay rate plot of parameters. By doing this, an easy tool is created for a machine designer to check the influence of each individual parameter on either the whirling speed or the decay rate.

4.3 Ordering

Taking a closer look at equation (30) and (31), the stability threshold speed only depends on the values of k, c_n, c_r, c_h and g. First of all, an important remark is that if c_r, or the scalar derived from the viscous damping of the shaft, is zero, the stability threshold speed becomes infinite, so the rotor is stable for all speeds. Secondly, if c_n, or the scalar derived from the non-rotating damping is large in comparison to c_r, the stability threshold speed can become very high. In practice this means that if the non-rotating damping is increased, by adding extra damping in the bearings, the stability threshold speed can easily be increased.
Although (30) will produce a value for every forward mode, only one will represent the stability threshold. Therefore, it would be very convenient if these values were ordered. This would mean that only the the stability threshold speed corresponding to the first forward mode is relevant. This kind of ordering is already known for the natural frequencies of an undamped, non-rotating system. This can be shown with Rayleigh's coefficient:

$$R(q) = \frac{\overline{\mathbf{q}}^T \mathbf{K} \mathbf{q}}{\overline{\mathbf{q}}^T \mathbf{M} \mathbf{q}} \tag{37}$$

with $\mathbf{K}$ and $\mathbf{M}$ being respectively the stiffness and the mass matrix of the system and $\mathbf{q}$ a vector variable. If $\mathbf{q}$ is replaced by the eigenvectors of the system, the corresponding eigenvalues are obtained and they are ordered

$$\omega_1^2 < \omega_2^2 < ... < \omega_n^2 \tag{38}$$

with n the degrees of freedom. This means that if the damping and gyroscopic effect in equation (14) is neglected, the same would hold for the scalars calculated by equation (21)

$$k_1 < k_2 < ... < k_n \tag{39}$$

There could be a similar way to express the damped rotating system. This could be true if there is a same conclusion for the scalars g, c_n,c_r and c_h. Consequently it can be seen from equation (30) and (31) that not only the whirling speeds are ordered, but also the stability threshold speeds. This means that

$$\Omega_{s1} < \Omega_{s2} < ... < \Omega_{sn} \tag{40}$$

or

$$\left[\omega_{si}\left(1+\frac{c_{ni}}{c_{ri}}\right)\pm\frac{c_{hi}}{c_{ri}}\right]<\left[\omega_{s(i+1)}\left(1+\frac{c_{n(i+1)}}{c_{r(i+1)}}\right)\pm\frac{c_{h(i+i)}}{c_{r(i+1)}}\right] \tag{41}$$

With Ω_{si} the stability threshold corresponding to the eigenvector of the i^{th} forward mode. However, the outcome of equations (21-22) are highly dependent on the structure of the individual matrices and the matrices depend on the modeling choice. Thus, an accurate estimate can only be derived by numerical calculation substantiated by experimental validation.

5 Numerical results

In order to illustrate the findings above, a numerical example, taken from [9], is used; i.e. a circular shaft with a diameter of 10.16 cm and a length of 127 cm supported by two identical bearings with a translational stiffness of 1.75×10^7 N/m. The shaft is considered to have a Young modulus of 2.07×10^7 Pa and a density of 7800 kg/m^3. The five parameters (21-25) that are used to visualize the difference between viscous damping, hysteretic damping and a combination of both are depicted by their effect on the stability threshold speed. Also, the decay rate plot of parameters is constructed.

5.1 Viscous damping

The shaft behaves purely viscously damped with a loss factor η_v of 0.0002. If the hysteretic loss factor is zero, then (30) and (31) reduce to

$$\Omega_s=\omega_s\left(1+\frac{c_n}{c_r}\right) \tag{42}$$

$$\omega_s=\pm\sqrt{\frac{k}{1+g\left(1+\frac{c_n}{c_r}\right)}} \tag{43}$$

If there is no damping in the bearings (Table 1), c_n is zero and the stability threshold speed equals the whirling speed. Because the whirling speeds are always ordered, the same ordering accounts for the stability threshold speeds. Nevertheless, all parameters are ordered except for c_r. Moreover, it can be seen that, if there is no damping in the bearings, and there is viscous damping in the shaft, the rotor will always be unstable when rotating above the first whirling speed. When the damping in both bearings is 100 Ns/m, a factor c_n appears (Table 2). Although the damping of the bearings is relatively high with respect to the damping in the shaft, the factor c_n is lower. This can be dedicated to the fact that the bearing damping is only active on two locations. As expected from (42), the stability threshold speed increases slightly. The ordering for the first three modes remains, so the stability threshold lies at 545.00 rad/s.
If the damping in the bearings is increased to 500 Ns/m (Table 3), all parameters stay the same, except for c_n. Taking a closer look to the relation between c_n and c_r, it can be seen that for the second mode c_n is bigger than c_r. This results in a quite big change of Ω_{s2} and consequently Ω_{s3} is smaller than Ω_{s2}. The ordering does not hold anymore. Nevertheless, this is of inferior importance because the stability threshold still is the lowest one, namely 636.30 rad/s. It should also be noted that the stability threshold of the first mode is very low with respect to the second one. This is related to the fact that the factor c_n of the first mode is also relatively low according to the second.

	c_n	c_r	c_h	g	k	$\Omega_s[rad/s]$	$\omega_s[rad/s]$
1	0	21.53	0	0.0013	2.72×10^5	522.17	522.17
2	0	18.90	0	0.0084	1.20×10^6	1.10×10^3	1.10×10^3
3	0	634.58	0	0.0364	5.06×10^6	2.29×10^3	2.29×10^3

Table 1: Parameters of the shaft with length 1.27m, $\eta_v = 0.0002$, $\eta_h = 0$ and no damping in the bearings

	c_n	c_r	c_h	g	k	$\Omega_s[rad/s]$	$\omega_s[rad/s]$
1	0.94	21.53	0	0.0013	2.72×10^5	545.00	522.18
2	6.33	18.90	0	0.0084	1.20×10^6	1.47×10^3	1.10×10^3
3	10.81	634.58	0	0.0364	5.06×10^6	2.33×10^3	2.29×10^3

Table 2: Parameters of the shaft with length 1.27m, $\eta_v = 0.0002$, $\eta_h = 0$ and a damping 100 Ns/m in both bearings

	c_n	c_r	c_h	g	k	$\Omega_s[rad/s]$	$\omega_s[rad/s]$
1	4.70	21.53	0	0.0013	2.72×10^5	636.30	522.26
2	31.65	18.91	0	0.0084	1.20×10^6	2.97×10^3	1.11×10^3
3	54.04	634.58	0	0.0364	5.06×10^6	2.49×10^3	2.30×10^3

Table 3: Parameters of the shaft with length 1.27m, $\eta_v = 0.0002$, $\eta_h = 0$ and a damping 500 Ns/m in both bearings

As for the decay rate plot of parameters, if only viscous damping is considered, straight lines can be seen rising towards zero. In Figure 3 and 4 with respectively zero damping and damping of 100 Ns/m in the bearings, plot one is also the first to reach instability and the second one follows. With 500 Ns/m damping in the bearings, however, plot three rise more rapidly than the second one, resulting in a lower stability threshold.

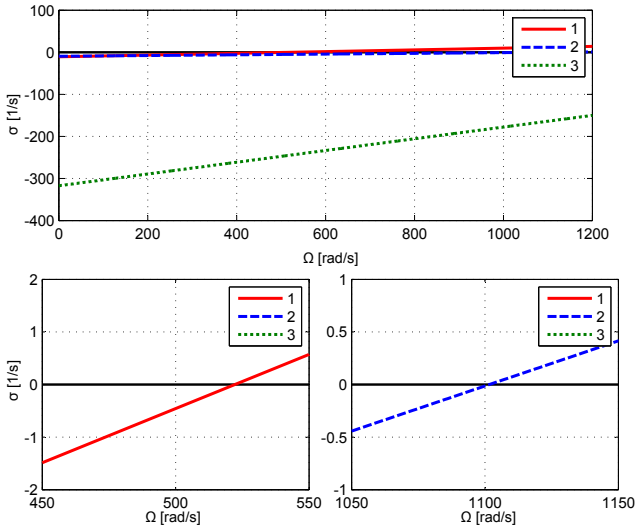

Figure 3: Decay rate plot of parameters of the shaft with length 1.27m, $\eta_v = 0.0002$, $\eta_h = 0$ and no damping in the bearings

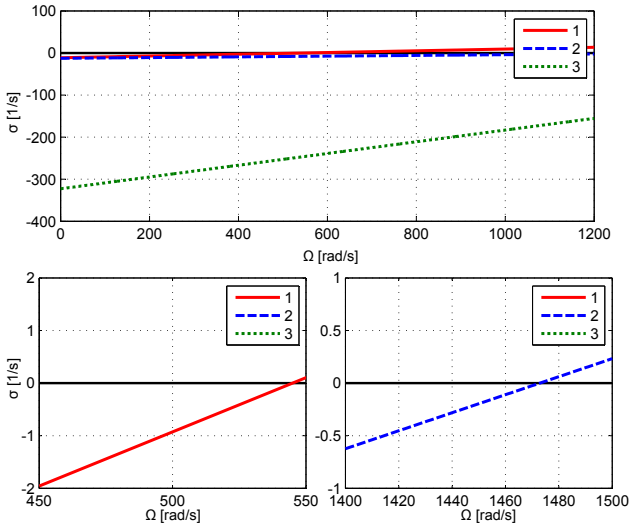

Figure 4: Decay rate plot of parameters of the shaft with length 1.27m, $\eta_v = 0.0002$, $\eta_h = 0$ and a damping 100 Ns/m in both bearings

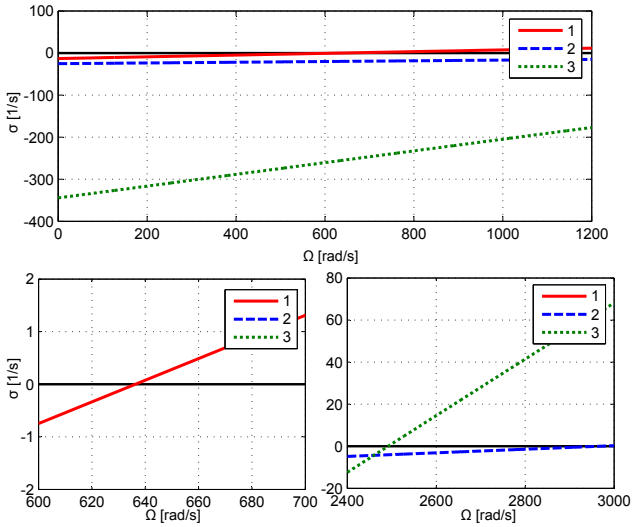

Figure 5: Decay rate plot of parameters of the shaft with length 1.27m, $\eta_v = 0.0002$, $\eta_h = 0$ and a damping 500 Ns/m in both bearings

5.2 Hysteretic damping

The shaft behaves purely hysteretically with a hysteretic loss factor of 0.0002. If the damping is purely hysteretic (30) and (31) can not be used, because σ is never zero. Therefore only the decay rate plot of parameters can give an answer. The decay rate is a constant, with a sudden discontinuity at every whirling speed. The difference with the viscous damping is remarkable. If there is no damping in the bearings, the stability threshold speed corresponds the viscous alternative (Figure 6), namely the first forward whirling speed 522.17 rad/s. Whenever the damping in the bearings is increased (Figure 7 and 8), the shaft is stable for all speeds.

5.3 Viscous and hysteretic damping combination

The shaft behaves both viscously and hysteretically with a loss factors η_v of 0.0002 and η_h of 0.0002. Equation (30) and (31) can be used. Except for the slight increase in the stability thresholds with respect to

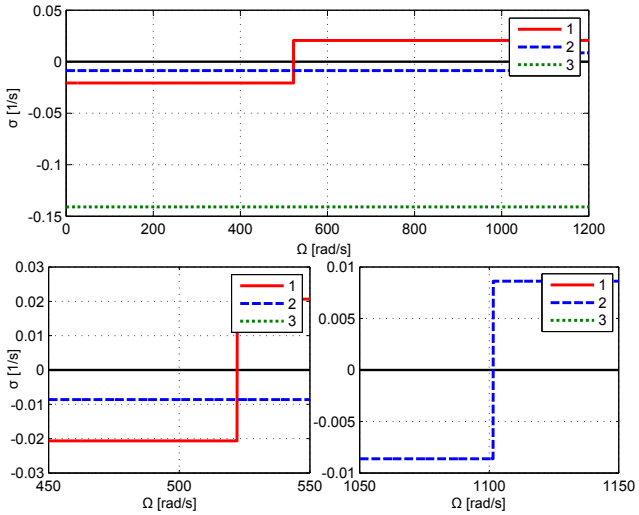

Figure 6: Decay rate plot of parameters of the shaft with length 1.27m, $\eta_v = 0$, $\eta_h = 0.0002$ and no damping in the bearings

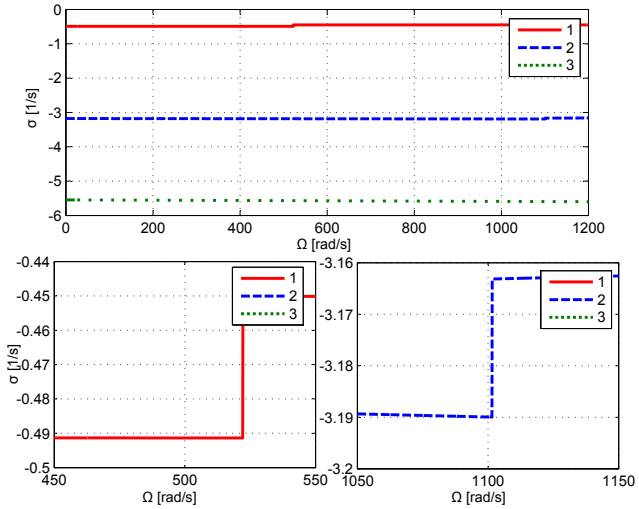

Figure 7: Decay rate plot of parameters of the shaft with length 1.27m, $\eta_v = 0$, $\eta_h = 0.0002$ and a damping 100 Ns/m in both bearings

the pure viscous damping, Tables 4,5 and 6 are practically the same. Therefore, the same conclusions can be made

	c_n	c_r	c_h	g	k	$\Omega_s[rad/s]$	$\omega_s[rad/s]$
1	0	21.53	21.53	0.0013	2.73×10^5	523.16	522.17
2	0	18.90	18.90	0.0084	1.20×10^6	1.10×10^3	1.10×10^3
3	0	634.58	634.58	0.0364	5.06×10^6	2.29×10^3	2.29×10^3

Table 4: Parameters of the shaft with length 1.27m, $\eta_v = \eta_h = 0.0002$ and no damping in the bearings

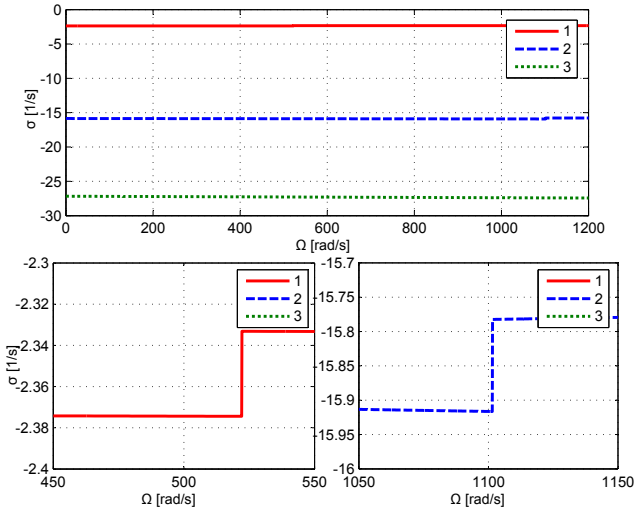

Figure 8: Decay rate plot of parameters of the shaft with length 1.27m, $\eta_v = 0$, $\eta_h = 0.0002$ and a damping 500 Ns/m in both bearings

	c_n	c_r	c_h	g	k	$\Omega_s[rad/s]$	$\omega_s[rad/s]$
1	0.9408	21.53	21.53	0.0013	2.72×10^5	546.00	522.18
2	6.33	18.90	18.90	0.0084	1.20×10^6	1.47×10^3	1.10×10^3
3	10.81	634.58	634.58	0.0364	5.06×10^6	2.33×10^3	2.29×10^3

Table 5: Parameters of the shaft with length 1.27m, $\eta_v = \eta_h = 0.0002$ and a damping 100 Ns/m in both bearings

	c_n	c_r	c_h	g	k	$\Omega_s[rad/s]$	$\omega_s[rad/s]$
1	4.70	21.53	21.53	0.0013	2.72×10^5	637.30	522.26
2	31.65	18.91	18.91	0.0084	1.20×10^6	2.97×10^3	1.11×10^3
3	54.04	634.58	634.58	0.0364	5.06×10^6	2.49×10^3	2.30×10^3

Table 6: Parameters of the shaft with length 1.27m, $\eta_v = \eta_h = 0.0002$ and a damping 500 Ns/m in both bearings

The decay rate plots of parameters are also very similar to the ones with the purely viscous damping (Figures 9-11), except for the discontinuity on the whirling speed. An important remark is that, whenever the shaft has a slight viscous behavior, there will be a certain speed at which the shaft will become unstable.

6 Conclusion

In rotating systems, the linear speed dependent model is a convenient way to describe its dynamic behavior. With these kind of models it is also possible to make an estimation of the stability threshold speed. By decoupling the system into a set of scalar equations, a straightforward description of the stability threshold is obtained depending on five parameters. Furthermore, the same parameters can be used to calculate the Campbell diagram and the decay rate plot. By doing this an easy tool is made for the machine designer to determine the influence of each parameter on the stability threshold speed. However, this stability threshold speed is highly dependent on the modeling choice and especially the modeling of damping. Mostly, in linear

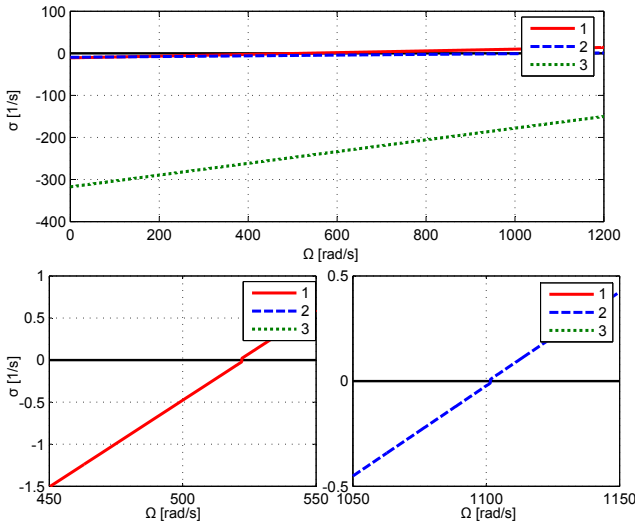

Figure 9: Decay rate plot of parameters of the shaft with length 1.27m, $\eta_v = 0.0002$, $\eta_h = 0.0002$ and no damping in the bearings

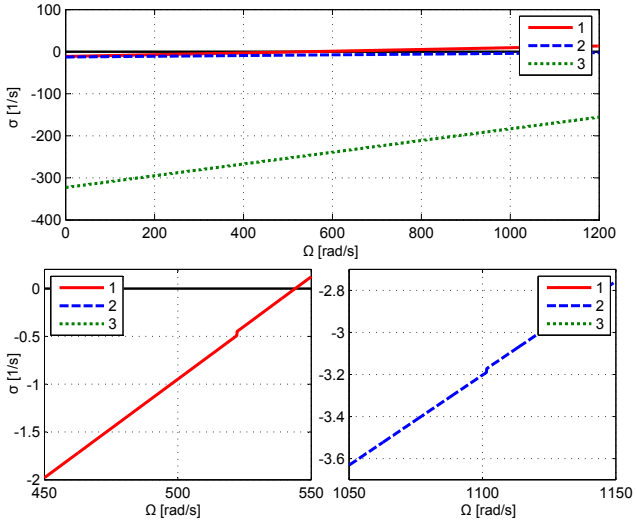

Figure 10: Decay rate plot of parameters of the shaft with length 1.27m, $\eta_v = 0.0002$, $\eta_h = 0.0002$ and a damping 100 Ns/m in both bearings

models either viscous damping, hysteretic damping or a combination of both is used. Whereas the hysteretic damping model has a better physical interpretation, it can only be used with harmonic motion. Apparently, for a rotor with hysteretic damping it could sometimes be concluded that the rotor is stable for all speeds while for the same rotor with viscous damping there will always be a stability threshold.
Not only the choice of the damping type affects the stability threshold, also the relation between the damping in the bearings and the damping in the shaft. For every forward mode, an equation can be composed each resulting in a certain threshold speed. Because it is impossible to rotate above this, only the lowest value is relevant. Consequently, if these threshold speeds were ordered, the lowest speed would always be the one corresponding the first mode. The numerical results in this paper agree with this statement, for this specific case. Although, it can also be seen that the ordering does not hold for all modes. Whenever the stability threshold speed of the first mode gets bigger than the second one, wrong conclusions could be made. In future research, a more thorough study of the parameters itself will be performed including a the influence of the bearing properties and locations, together with the influence on the ordering. Also, the results will be verified with an experimental validation.

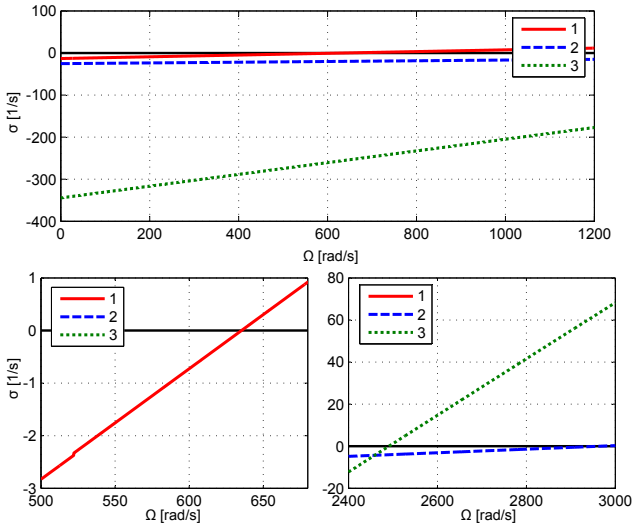

Figure 11: Decay rate plot of parameters of the shaft with length 1.27m, $\eta_v = 0.0002$, $\eta_h = 0.0002$ and a damping 500 Ns/m in both bearings

References

[1] ML Adams and J. Padovan. Insights into linearized rotor dynamics. *Journal of Sound and Vibration*, 76(1):129–142, 1981.

[2] Mohamed A Kandil. *On Rotor Internal Damping Instability*. PhD thesis, 2004.

[3] L Forrai. Instability due to internal damping of symmetrical rotor-bearing systems. *JCAM*, 1(2):137–147, 2000.

[4] Giancarlo Genta. *Dynamics of rotating systems, Volume 1*. Springer, 2005.

[5] Karl Meerbergen. The quadratic eigenvalue problem Problem . *Society*, 2006.

[6] I. Bucher and D. J. Ewins. Modal analysis and testing of rotating structures. *Philosophical Transactions of the Royal Society A: Mathematical, Physical and Engineering Sciences*, 359(1778):61–96, January 2001.

[7] Enrique Simon Gutierrez-Wing. Modal analysis of rotating machinery structures, January 2003.

[8] Maurice L. Adams. *Rotating machinery vibration: from analysis to troubleshooting*. CRC Press/Taylor & Francis, 2009.

[9] E. S. Zorzi and H. D. Nelson. Finite Element Simulation of Rotor-Bearing Systems With Internal Damping. *Journal of Engineering for Power*, 99(1):71–76, January 1977.

[10] G RAMANUJAM and C BERT. Whirling and stability of flywheel systems, part I: Derivation of combined and lumped parameter models. *Journal of Sound and Vibration*, 88(3):369–398, June 1983.

[11] Giancarlo Genta and Nicola Amati. Hysteretic damping in rotordynamics: An equivalent formulation. *Journal of Sound and Vibration*, 329(22):4772–4784, October 2010.

[12] L. Junfeng and Wang Zhaolin. Stability of non-conservative linear gyroscopic systems. *Applied Mathematics and Mechanics*, 17(12):1171–1175, 1996.